Acta Astronautica 225 (2024) 390–401

Contents lists available at ScienceDirect

Acta Astronautica

journal homepage: www.elsevier.com/locate/actaastro

Optimization of MMX relative quasi-satellite transfer trajectories using primer vector theory

Nishanth Pushparaj [a,*], Nicola Baresi [b], Yasuhiro Kawakatsu [c]

[a] Nottingham Geospatial Institute, University of Nottingham, Nottingham, NG7 2RD, United Kingdom
[b] Surrey Space Centre, The University of Surrey, Guildford, Surrey, GU2 7XH, United Kingdom
[c] Institute of Space and Astronautical Sciences, Japan Aerospace Exploration Agency, Sagamihara, Japan

ARTICLE INFO

Keywords:
CRTBP
Primer vector theory
Quasi-satellite orbits
Martian Moons exploration
Optimal control

ABSTRACT

Quasi-satellite orbits (QSO) are stable retrograde parking orbits around Phobos that are currently being considered for JAXA's upcoming robotic sample return mission Maritan Moons Exploration (MMX). During the proximity operations of MMX, the spacecraft inserted in a high altitude QSO will gradually descend to lower altitude QSOs with suitable transfer and station-keeping techniques between different relative QSOs. Preliminary analysis of two-impulsive planar transfers between relative retrograde orbits utilizing the bifurcated QSOs families is studied to estimate the ΔV costs and time of flights of the transfers. In this paper, differently from previous works, we utilize the initial guesses found through the preliminary results that provide two-impulsive transfer ΔV execution points and optimize the transfers between relative QSOs around Phobos. Primer vector theory is applied to investigate the primer vector of the MMX transfer trajectories to evaluate whether intermediate maneuver or initial/final coasting times along the trajectories can minimize the total ΔV cost between the transfers. Based on the primer vector analysis of the impulse transfer trajectories, it is found that departing and arriving at the same periphobian sides with an additional mid-course impulse results in the optimal impulse solution.

1. Introduction

Martian Moons eXploration (MMX) mission is JAXA's upcoming robotic sample return mission to explore the two moons of Mars, Phobos and Deimos. The primary scientific objective of the MMX mission is to settle speculations on the origin of these planetary satellites, eventually solving the mysteries of planetary formation in the Solar system [1,2]. The engineering objective of MMX includes technology demonstration of round-trips between Earth-Mars, sampling techniques over the surface of the Martian moon. MMX is currently scheduled for a 2024 launch, starting with the interplanetary and Mars Orbit Insertion (MOI) phase, followed by a three-year-long Phobos Proximity Phase (PP) to perform sample retrieval operations and scientific observations of Phobos and finally return samples to Earth by 2029 [3,4].

The dynamical environment around Phobos is unique compared to other Planetary systems [5]. In the Mars-Phobos system, Phobos has a sphere of influence embedded within its surface due to its smaller mass, density, and proximity to Mars. A simple two-body approximation with Mars is not appropriate to describe the dynamics in the vicinity of Phobos. To ensure the safe operation of the spacecraft in the proximity of Phobos for a more extended mission period, MMX envisions utilizing relative Quasi-Satellite Orbits (QSOs) to characterize the gravitational field of Phobos before landing operations.

This research primarily focused on the transfer problem between the QSOs in the Phobos proximity phase of the MMX mission. During its proximity phase around Phobos, MMX will transfer between QSO orbits to change its altitude relative to the Martian moon's surface. To this end, Ichinomiya et al. [6] and Pushparaj et al. [7] investigated the application of in-plane bifurcated multi-revolution QSOs to develop transfer trajectories between MMX baseline QSOs. Liang et al. [8] developed an approach to facilitate point-to-point jumping transfers on the surface of Phobos for the MMX mission, effectively overcoming the challenges posed by its irregular terrain. Canalias et al. [9], Chen et al. [10] and Pushparaj et al. [11,12] further explored transfers to out-of plane QSOs using two-impulse maneuvers and invariant manifolds, respectively.

This paper optimizes transfers between MMX candidate QSOs using the results of previous transfer analysis as an initial guess, which provides two-impulse transfer ΔV execution points. In addition, we use primer vector theory, an indirect optimization method based on the calculus of variations and optimal control theory to validate the

* Corresponding author.
E-mail address: nishanth.pushparaj@nottingham.ac.uk (N. Pushparaj).

https://doi.org/10.1016/j.actaastro.2024.09.031
Received 2 July 2024; Received in revised form 6 September 2024; Accepted 13 September 2024
Available online 18 September 2024

results [13,14]. Primer vector theory (PVT) uses the costate velocity vector to evaluate if a trajectory satisfies the necessary analytical conditions for optimality. If the necessary conditions are not satisfied, the theory indicates how the candidate trajectory should be modified to reduce its transfer cost, such as adding an initial or final coast, a midcourse impulse, or changing the timing, magnitude, and direction of an already existing midcourse impulse, respectively [15,16].

Prussing and Chiu's work highlights the use of PVT to calculate the optimal number of impulses, their precise timings, placements, and the strategic inclusion of coasting arcs either at the beginning or end of the maneuvers [17]. Casalino et al. [18] extended the use of PVT to scenarios involving impulsive maneuvers, such as planetary flybys and arrivals. Zhu et al. [19] utilized PVT to streamline and enhance the trajectory planning process, involving three impulses. Li et al. [20] explored the optimal transfer trajectory design for interplanetary missions involving planetary escape and capture phases in heliocentric frames. Hiday-Johnston and Howell expanded the scope of PVT by adapting it to the elliptical restricted three-body problem, enhancing the theory's applications to more complex orbital environments more specifically to the optimal time-fixed trajectories between three-dimensional liberation point orbits for Sun-Earth-Moon systems [21]. Davis et al. [22] applied PVT to develop optimal maneuvers that facilitate the creation of a bridging transfer arc, connecting unstable and stable manifold trajectories. Bokelmann and Russell's investigation into optimizing impulsive transfer trajectories for Europa capture demonstrates PVT's utility in minimizing the costs associated with complex orbital insertions in the Jupiter-Europa system [23]. Jezewski [24] utilized the PVT method to analyze the Clohessy-Wiltshire equations, which define the relative motion of the satellite to a circular reference orbit. Shuster et al. [25] introduced analytical solutions for maneuver sequences affecting safety ellipse operations, employing PVT to derive relationships between trajectory optimality and the geometrical properties of the initial and final safety ellipses. Zheng et al. [26] utilized PVT to enhance the relative motion of arbitrary elliptical reference orbits within target orbital coordinate systems. Bucchioni et al. [27] applied PVT to study optimal time-fixed impulsive transfer trajectories connecting two non-keplerian orbits, more specifically in the Earth-Moon CRTBP framework. Rebelo and Sanchez conducted a study on optimizing the trajectory using PVT [28]. They specifically focused on intercept trajectories, including many revolutions and deep space maneuvers in the context of ESA's Comet Interceptor mission. Though PVT is not a new concept for space trajectory optimization, it has proven to be a useful tool in optimizing trajectories in the existing literature. Differently from previous studies, this research focuses on developing a PVT formulation for the Circular Hill Problem with an ellipsoidal secondary model and more specifically, it is applied to the Mars-Phobos system to support the selection of delta V execution points for the proximity operations of the MMX mission.

This paper is organized as follows. Section 2 introduces the dynamical model and equations of motion used in this work along with numerical computation of QSOs. This work considers the Circular Hill Problem with the Ellipsoidal Secondary (Mars-Phobos system). Section 3 presents the Impulsive Primer Vector Theory, the optimization process, and the background. Section 4 summarizes the transfer methodology utilizing bifurcated QSOs and the initial guess generation for the optimization process. Finally, Section 5 provides the trajectory optimization results for MMX baseline orbits, followed by Section 6, key findings and conclusions from this research.

2. Dynamical model

The general problem of satellite and particle dynamics about a tri-axial ellipsoid with a constant density model is considered. The tri-axial ellipsoidal model of Phobos can be framed by specifying the physical parameters of the smaller body as follows. The largest semi-major axis always points along the x-axis, the intermediate semi-major axis along the y-axis, and the smallest semi-major axis along the z-axis, as shown in Fig. 1. It is assumed that Phobos orbits around Mars in a tidally-locked configuration. Accordingly, the tri-axial ellipsoid representing the surface of the Martian moon does not rotate with respect to the Mars-Phobos synodic reference frame.

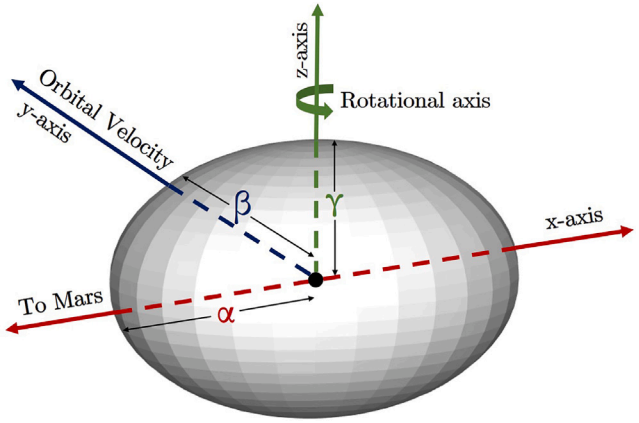

Fig. 1. Tri-axial ellipsoid $\gamma \leq \beta \leq \alpha$.

Table 1
Phobos physical properties.

Properties	Values
α, Largest semi-major axis	13.03 km
β, Intermediate semi-major axis	11.4 km
γ, Smallest semi-major axis	9.14 km
σ_P, Density	1.860 g/cm^3
μ_P, Gravitational parameter	0.000706 km^3/s^2
M_P, Mass	1.058×10^{16} kg
a_P, Phobos semi-major axis	9377 km
P_P, Rotational period	7.66 hr
ω_P, Spin rate	2.279×10^{-4} rad/s

2.1. Model specifications

The irregular gravity field of Phobos can be approximated using an ellipsoidal model with three major axes: α, β, and γ as shown in Fig. 1. Assuming constant density σ_P, the gravitational parameter of Phobos is computed as [29,30]

$$\mu_P = \frac{4\pi}{3} G \sigma_P \alpha \beta \gamma, \tag{1}$$

where G, is the gravitational constant 6.674×10^{-8} cm^3 g^{-1} s^{-2} and $\frac{4\pi}{3}\alpha\beta\gamma$ is the volume of the ellipsoid. The gravitational potential of a constant density tri-axial ellipsoidal Phobos model at a point x, y, z, is given by

$$\mathcal{U}(x, y, z) = -\mu_P \frac{3}{4} \int_0^\infty \phi(x, y, z, u) \frac{dl}{\Delta(l + \Lambda)}, \tag{2}$$

where

$$\phi(x, y, z, l + \Lambda) = \frac{x^2}{\alpha^2 + l + \Lambda} + \frac{y^2}{\beta^2 + l + \Lambda} + \frac{z^2}{\gamma^2 + l + \Lambda} - 1, \tag{3}$$

$$\Delta(l + \Lambda) = \sqrt{(\alpha^2 + l + \Lambda)(\beta^2 + l + \Lambda)(\gamma^2 + l + \Lambda)}. \tag{4}$$

μ_P is the gravitational parameter of Phobos from the Eq. (1), whereas Λ is defined as either to be zero or the real positive root of $\phi(x, y, z, l + \Lambda) = 0$, depending on whether the gravitational attraction of Phobos is computed internally or externally of the body. Physical properties of Phobos are provided in Table 1[31].

2.2. Equations of motion

The dynamical model used in this study is based on the Circular Hill problem, which simplifies the restricted three-body (R3BP) by assuming

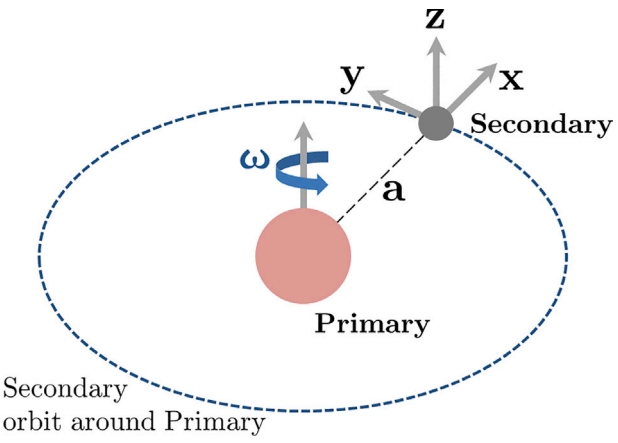

Fig. 2. Hill problem.

a small mass ratio between the primary and secondary bodies, in this case, Mars and Phobos. Since the gravitational parameter of Phobos is significantly smaller than the gravitational parameter of Mars and the relative distance between spacecraft and Phobos is significantly smaller than the distance between Mars and its moons, the differential equations governing the motion of mass particles around Phobos can be well approximated via the Hill approximation of the Circular Restricted Three-Body Problem (CRTBP) given by [32,33]. Given the extreme mass ratio and the spacecraft's proximity to Phobos, this approach captures the general dynamics near Phobos while maintaining computational efficiency. Additionally, we incorporate Phobos's non-spherical, ellipsoidal shape to account for its gravitational irregularities, which provides better fidelity in modeling the local perturbations than a purely spherical model.

The Hill Problem's equations of motion are defined in a rotating reference frame centered at the secondary's barycenter as shown in Fig. 2, where, x-axis parallel to the line connecting the primary and secondary bodies, the z-axis parallel to the orbital angular momentum vector, and the y-axis in the direction of orbital velocity of the secondary.

$$\begin{cases} \ddot{x} - 2\dot{y} &= g_x + 3\,x, \\ \ddot{y} + 2\dot{x} &= g_y, \\ \ddot{z} &= g_z - z, \end{cases} \tag{5}$$

where $G_a = [g_x, g_y, g_z]^T$ is the normalized acceleration due to an attracting ellipsoidal mass and it is given by,

$$g_x = -\frac{3}{2}\mu_P x \int_0^\infty \left(\frac{1}{\alpha^2 + l + \Lambda}\right) \frac{dl}{\Delta(l+\Lambda)}, \tag{6}$$

$$g_y = -\frac{3}{2}\mu_P y \int_0^\infty \left(\frac{1}{\beta^2 + l + \Lambda}\right) \frac{dl}{\Delta(l+\Lambda)}, \tag{7}$$

$$g_z = -\frac{3}{2}\mu_P z \int_0^\infty \left(\frac{1}{\gamma^2 + l + \Lambda}\right) \frac{dl}{\Delta(l+\Lambda)}. \tag{8}$$

Eqs. (2) and (6–8) are elliptic integrals which can be rapidly approximated using numerical procedures [34]. It is also worth noting that the equations of motion Eq. (5) admit an integral of motion known in the literature as the Jacobi integral and expressed as

$$C = \mathcal{W}(\boldsymbol{r}) - \frac{1}{2}(\dot{x}^2 + \dot{y}^2 + \dot{z}^2), \tag{9}$$

where $\mathcal{W}(\boldsymbol{r}) = \frac{1}{2}(3\,x^2 - z^2) + \mathcal{U}(x, y, z)$ is the effective potential of the system. Since $\mathcal{T} = \frac{1}{2}(\dot{x}^2+\dot{y}^2+\dot{z}^2) = \mathcal{W}-C \geq 0$, the Jacobi integral divides the vicinity of Phobos in areas of forbidden and admissible motion. where $\mathcal{U}(x, y, z)$ is the normalized acceleration due to an attracting ellipsoidal mass. Key dynamic properties of distant retrograde orbits or quasi-satellite orbits (QSO) will be reviewed in the next subsection.

Table 2
Specifications of MMX baseline QSO.

Name	$x \times y$ (km)	$\dot{x} \times \dot{y}$ (m/s)	T(h)
QSO-H	100×198.47	45.74×22.95	7.59
QSO-M	50×94.41	23.41×12.04	7.13
QSO-La	30×48.83	15.31×8.68	5.76
QSO-Lb	22×30.81	12.79×8.25	4.40
QSO-Lc	20×26.69	12.31×8.31	3.97

While this formulation serves the context of this study, conclusions drawn about the optimal ΔV and transfer design should hold qualitatively when applied to more complex models such as the Elliptic Restricted Three-Body Problem (ER3BP) or even higher-fidelity ephemeris models. However, additional perturbations in those models may alter the specific quantitative results. Future work could expand on these findings by comparing transfer trajectories under more realistic dynamical models.

2.3. Planar and spatial QSOs

QSOs are retrograde periodic orbits existing around the smaller primary. In this research, we have utilized pseudo-arclength continuation method of Mittelmann [35] and shooting methods for calculating families of QSO as shown in Fig. 3. QSOs are highly energetic trajectories reaching up to the surface of Phobos. The current mission design of MMX envisages the utilization of different altitude planar QSOs in order to characterize the gravitational field before landing on Phobos. Key features of these baseline trajectories are tabulated in Table 2, whereas Fig. 4 depicts the candidate relative orbits as seen from the Mars-Phobos synodic frame [36].

The QSO family branch obtained through the pseudo-arclength continuation method is shown in Fig. 5 with the stability indices of the QSO family branch computed from Eq. (10).

$$b_j \equiv \lambda_j + \frac{1}{\lambda_j}, \quad j = 1, 2. \tag{10}$$

As shown by the linear analysis indicated by the stability indices of the QSO monodromy matrix eigenvalues, these relative orbits are linearly stable (i.e., when stability index $b_j > 2$). In a Hamiltonian system, the monodromy matrix of a periodic orbit, M $(d\Phi(x,T)/dx)$ is the state transition matrix of a periodic orbit after one time period and has three pairs of eigenvalues with one trivial pair $D = 1$. We bifurcate the planar QSO family using their stability indices defined as in Eq. (10) [37], where λ_j and $1/\lambda_j$ are jth reciprocal eigenvalues pairs of monodromy matrix, M.

$$b_{Res} = 2\cos 2\pi \frac{d}{n}, \quad d, n \in N. \tag{11}$$

Important characteristics of stability indices are when it reaches any resonant value (d/n), and the state corresponds to a bifurcation point indicated using the Eq. (11)[38,39]. Periodic orbits bifurcating via in-plane perturbations are *swing QSOs* or *MP-QSOs*, and the members bifurcating from out-of-plane perturbations are *3D-QSOs*. An example of in-plane bifurcated orbit of $(d/n) = 1/4$ and out-of-plane bifurcated orbits of $(d/n) = 1/6$ is shown within Fig. 5.

3. Impulsive primer vector theory

Primer vector theory (PVT) is an indirect method of optimizing transfer trajectories with necessary conditions and sufficient conditions (if available) derived from the indirect optimization of the fuel-minimum problem. When impulsive transfer trajectories are used, the primer vector determines the timing and location of thrust impulses in order to minimize propellant cost. PVT for impulsive transfer trajectories indicates whether adding a terminal coasting period and incorporating mid-course impulses or maneuvers can reduce the cost.

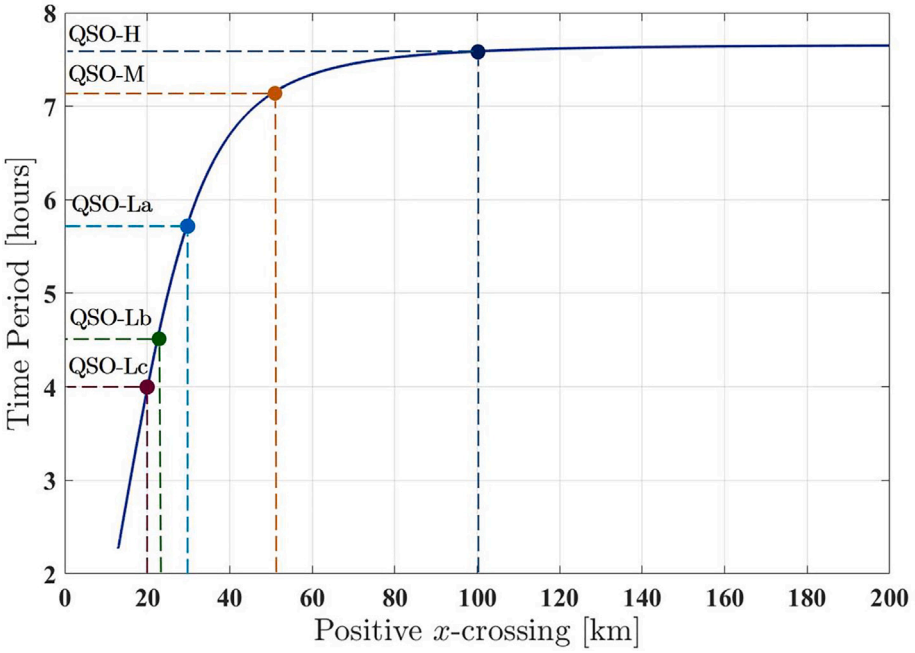

Fig. 3. Time period vs. positive x-axis crossing of the QSO family branch.

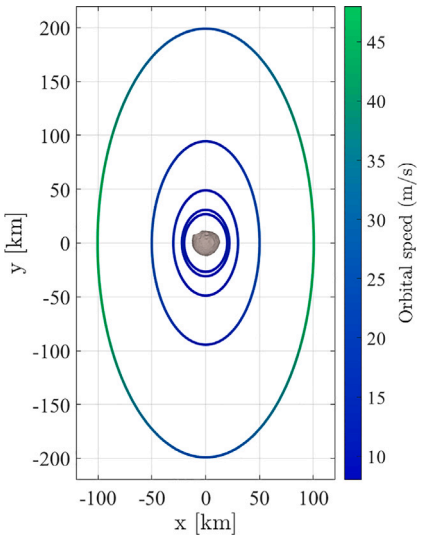

Fig. 4. MMX baseline QSOs.

For impulsive transfer, cost function representing minimum total ΔV can be defined as

$$J = \sum_{n=0}^{N} \Delta V_n, \tag{12}$$

Initial deviations to the reference trajectory ($\delta \dot{\boldsymbol{x}}$) can be linearly mapped to specific time using the state transition matrix (STM) $\Phi(t, t_0)$ as

$$\delta \dot{\boldsymbol{x}} = \begin{bmatrix} \delta \dot{\boldsymbol{r}} \\ \delta \dot{\boldsymbol{v}} \end{bmatrix} = \begin{bmatrix} O_3 & I_3 \\ G & K \end{bmatrix} \begin{bmatrix} \delta \boldsymbol{r} \\ \delta \boldsymbol{v} \end{bmatrix}, \tag{13}$$

where O_3 is 3×3 zero matrix, I_3 is 3×3 identity matrix, $G = G_r + C_f$, where G_r is 3×3 gravity gradient matrix, C_f is 3×3 centrifugal contributions from Eq. (5), and K is 3×3 Corolis contributions from Eq. (5). The elements of G_r are given by

$$g_{ij} = \partial^2 \Phi / \partial x_i \partial x_j, \tag{14}$$

Eq. (13) can be written in second-order form as

$$\delta \ddot{\boldsymbol{r}} = G \delta \boldsymbol{r} + K \delta \dot{\boldsymbol{r}}, \tag{15}$$

STM of this system can be partitioned in to four 3×3 matrices as follows:

$$\Phi(t, t_0) \equiv \begin{bmatrix} \Phi_A(t, t_0) & \Phi_B(t, t_0) \\ \Phi_C(t, t_0) & \Phi_D(t, t_0) \end{bmatrix}, \tag{16}$$

In order to minimize the cost function, we form Hamiltonian of the system, H using,

$$H = J + \lambda_r^T \dot{\boldsymbol{r}} + \lambda_v^T \dot{\boldsymbol{v}}, \tag{17}$$

where $\dot{\boldsymbol{r}}$ and $\dot{\boldsymbol{v}}$ are velocity and acceleration of the spacecraft, and λ_r^T and λ_v^T are 3×1 vector Lagrange multipliers that includes the equations of motion as non-linear constraints for the optimization problem.

The adjoint system to Eq. (13) is

$$\begin{bmatrix} \dot{\lambda}_r \\ \dot{\lambda}_v \end{bmatrix} = \begin{bmatrix} -K & -G \\ -I_3 & O_3 \end{bmatrix} \begin{bmatrix} \lambda_r \\ \lambda_v \end{bmatrix}, \tag{18}$$

Rewriting Eq. (18) in second-order form as

$$\ddot{\boldsymbol{\lambda}}_{\boldsymbol{v}} = G \boldsymbol{\lambda}_{\boldsymbol{v}} + K \dot{\lambda}_v, \tag{19}$$

is identical to Eq. (15), therefore STM for $(\lambda_{\boldsymbol{v}}, \dot{\lambda_{\boldsymbol{v}}})$ will be identical to Eq. (16)

$$\begin{bmatrix} \lambda_{\boldsymbol{v}}(t) \\ \dot{\lambda}_{\boldsymbol{v}}(t) \end{bmatrix} = \Phi(t, t_0) \begin{bmatrix} \lambda_{\boldsymbol{v}}(t_0) \\ \dot{\lambda}_{\boldsymbol{v}}(t_0) \end{bmatrix}, \tag{20}$$

Lawden [16] termed λ_v as the "primer vector" (i.e., $\lambda_v = \mathbf{p}$) and derived following necessary conditions for an optimal impulsive transfer trajectory.

- Primer vector and its derivative are continuous along the transfer trajectory.
- Primer vector magnitude satisfies $p(t) \leq 1$ with the ΔV impulses taking place at instants at which $p(t) = 1$.
- At impulse times, the primer vector is a unit vector in the optimal thrust direction.
- As a consequence of above conditions, $dp/dt = \dot{p} = \dot{\boldsymbol{p}}^T \boldsymbol{p} = 0$ at an intermediate impulse.

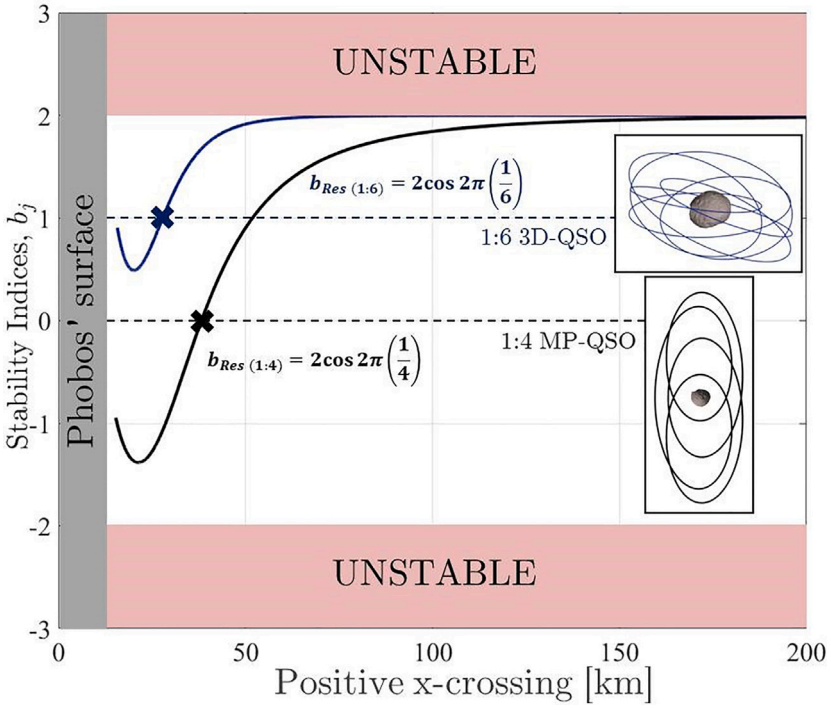

Fig. 5. Stability indices of planar QSO families.

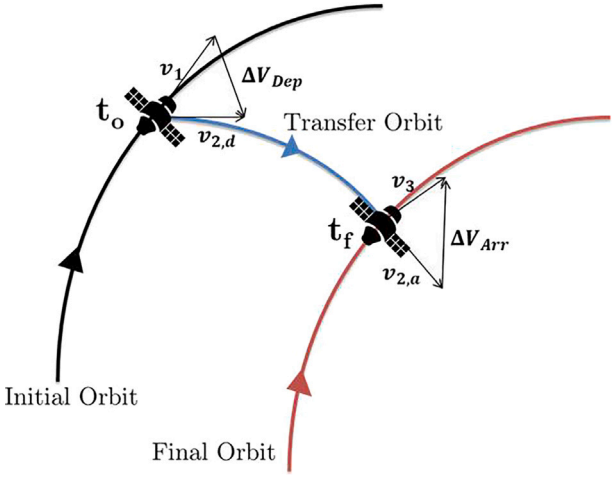

Fig. 6. Illustration of a two-impulse transfer trajectory.

In linear systems, these necessary conditions are also the sufficient conditions for an optimal trajectory.

Let $\boldsymbol{\Delta V}_{Dep}$ and $\boldsymbol{\Delta V}_{Arr}$ be the change in velocity at initial and terminal QSOs as illustrated in Fig. 6.

To satisfy the necessary conditions for an optimal trajectory, we can impose following boundary conditions on the primer vector

$$\boldsymbol{p}(t_0) \equiv \boldsymbol{p}_0 = \frac{\boldsymbol{\Delta V}_{Dep}}{\Delta V_{Dep}}, \tag{21}$$

$$\boldsymbol{p}(t_f) \equiv \boldsymbol{p}_f = \frac{\boldsymbol{\Delta V}_{Arr}}{\Delta V_{Arr}}, \tag{22}$$

From Eq. (20), the primer vector can then be evaluated along the transfer orbit using a 6×6 state transition matrix solution,

$$\begin{bmatrix} \boldsymbol{p}(t) \\ \dot{\boldsymbol{p}}(t) \end{bmatrix} = \boldsymbol{\Phi}(t, t_0) \begin{bmatrix} \boldsymbol{p}(t_0) \\ \dot{\boldsymbol{p}}(t_0) \end{bmatrix}, \tag{23}$$

From Eq. (23) and Eq. (16) primer vector and its derivative at time $[t_0\ t_f]$ evaluated as

$$\boldsymbol{p}_f = \boldsymbol{\Phi}_A(t_f, t_0)\boldsymbol{p}_0 + \boldsymbol{\Phi}_B(t_f, t_0)\dot{\boldsymbol{p}}_0, \tag{24}$$

$$\dot{\boldsymbol{p}}_f = \boldsymbol{\Phi}_C(t_f, t_0)\boldsymbol{p}_0 + \boldsymbol{\Phi}_D(t_f, t_0)\dot{\boldsymbol{p}}_0, \tag{25}$$

From Eq. (24), we have initial primer vector derivative as

$$\dot{\boldsymbol{p}}_0 = \boldsymbol{\Phi}_B^{-1}(t_f, t_0)[\boldsymbol{p}_f - \boldsymbol{\Phi}_A(t_f, t_0)\boldsymbol{p}_0], \tag{26}$$

knowing primer vector and its derivative at the initial time, one can evaluate the primer vector along the transfer trajectory between $[t_0\ t_f]$ using

$$\dot{\boldsymbol{p}}(t) = \boldsymbol{\Phi}_B(t, t_0)\boldsymbol{\Phi}_B^{-1}(t_f, t_0)\boldsymbol{p}_f + [\boldsymbol{\Phi}_A(t, t_0) - \boldsymbol{\Phi}_B(t, t_0)\boldsymbol{\Phi}_B^{-1}(t_f, t_0)\boldsymbol{\Phi}_A(t_f, t_0)]\boldsymbol{p}_0. \tag{27}$$

3.1. Criterion for adding terminal coast

Fig. 7 illustrates perturbed transfer orbit with impulses occurring at time $t_0 + dt_0$ due to initial coasting in the initial orbit of duration $dt_0 > 0$ and that final impulse occurring at a time $t_f + dt_f$. In the case of the final coast $dt_f < 0$, the final impulse occurs before the nominal final time, allowing a coast in the final orbit until the nominal final time. Note that a negative value of dt_0 or a positive value of dt_f also has a physical interpretation of whether coasting would lower the transfer cost of the trajectory. Suppose, the nominal initial transfer trajectory is

$$J = \Delta V_{Dep} + \Delta V_{Arr}, \tag{28}$$

In order to determine the differential change in the transfer cost due to the coasting periods the concept of noncontemporaneous variation is needed. This variation combines two effects: the variation due to being on a perturbed trajectory and the variation due to the difference in the time of the impulses. Based on [15], the rule for relating these two types of contemporaneous and noncontemporanerous variations is given by

$$d\boldsymbol{x}(t_0) = \delta\boldsymbol{x}(t_0) + \dot{\boldsymbol{x}}_{\boldsymbol{0}}^{*} dt_0, \tag{29}$$

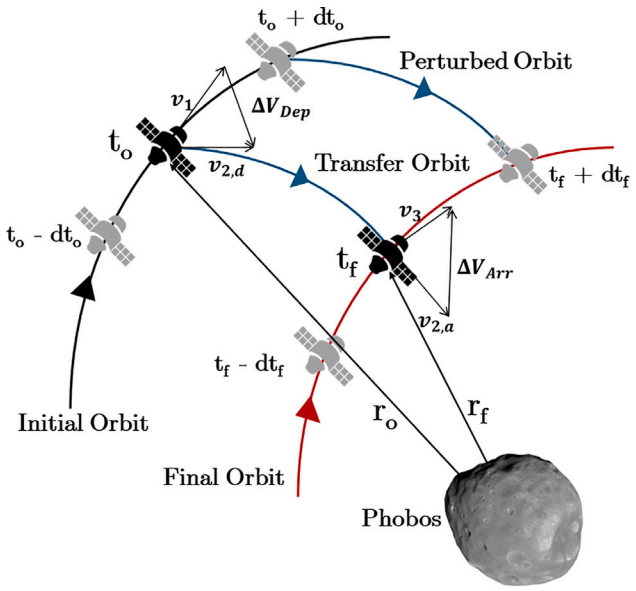

Fig. 7. Illustration of a two-impulse transfer trajectory with terminal coasts dt_0 and dt_f.

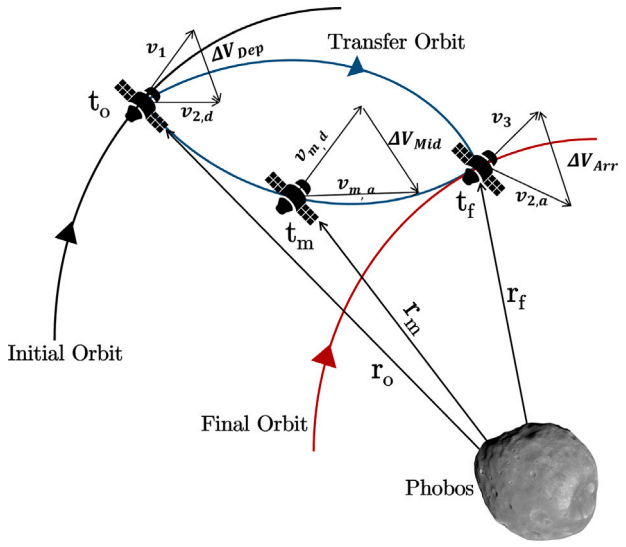

Fig. 8. Illustration of a two-impulse transfer trajectory with midcourse impulses.

where d and δ denote noncontemporaneous and contemporaneous variations respectively; $\boldsymbol{x}_0^*$ is the derivative on the nominal initial transfer trajectory at the nominal time and considers variations in the initial state as an initial guess.

Variation in the transfer cost can be expressed, from Eq. (28) as

$$dJ = \frac{\delta \Delta V_{Dep}}{\delta \boldsymbol{\Delta V}_{Dep}} d\boldsymbol{\Delta V}_{Dep} + \frac{\delta \Delta V_{Arr}}{\delta \boldsymbol{\Delta V}_{Arr}} d\boldsymbol{\Delta V}_{Arr}, \tag{30}$$

Eq. (30) can be expressed as

$$dJ = \frac{\boldsymbol{\Delta V}_{Dep}^T}{\Delta V_{Dep}} d\boldsymbol{\Delta V}_{Dep} + \frac{\boldsymbol{\Delta V}_{Arr}^T}{\Delta V_{Arr}} d\boldsymbol{\Delta V}_{Arr}, \tag{31}$$

Now, the Eq. (31) can be rewritten in terms of the initial and final primer vector using the Eqs. (21)–(22) as

$$dJ = \boldsymbol{p}_0^T d\boldsymbol{\Delta V}_{Dep} + \boldsymbol{p}_f^T d\boldsymbol{\Delta V}_{Arr}, \tag{32}$$

Furthermore, the analysis from [15] leads to

$$dJ = -\dot{\boldsymbol{p}}_0^T \boldsymbol{\Delta V}_{Dep} dt_0 + \dot{\boldsymbol{p}}_f^T \boldsymbol{\Delta V}_{Arr} dt_f, \tag{33}$$

$$dJ = -\Delta V_{Dep} \dot{\boldsymbol{p}}_0^T \boldsymbol{p}_0 dt_0 - \Delta V_{Arr} \dot{\boldsymbol{p}}_f^T \boldsymbol{p}_f dt_f, \tag{34}$$

Eq. (34) gives the gradients of the cost function with respect to terminal impulse times t_0 and t_f as

$$\frac{\partial J}{\partial t_0} = -\Delta V_{Dep} \dot{\boldsymbol{p}}_0^T \boldsymbol{p}_0, \tag{35}$$

and

$$\frac{\partial J}{\partial t_f} = -\Delta V_{Arr} \dot{\boldsymbol{p}}_f^T \boldsymbol{p}_f, \tag{36}$$

Note that the Eqs. (35)–(36) are simply the slopes of primer magnitude time history at the terminal times, due to the fact $p^2 = \boldsymbol{p}^T \boldsymbol{p}$, and after differentiation with time, $2p\dot{p} = 2\dot{\boldsymbol{p}}^T \boldsymbol{p}$.

$$\dot{\boldsymbol{p}}^T \boldsymbol{p} = \frac{dp}{dt}, \tag{37}$$

Lion and Handelsman [15] proposed specific criterion that satisfy the necessary conditions for optimality when two-impulse transfer trajectories fail to satisfy the necessary conditions. Criterion for adding terminal coasts/earlier impulses are listed as follows:

1. If $\dot{p}_0 > 0$, an initial coast will lower the transfer cost. Similarly, if $\dot{p}_f < 0$, a final coast will lower the cost.
2. If $\dot{p}_0 < 0$, implying an earlier impulse time would lower the cost (i.e., starting the transfer earlier). Likewise, $\dot{p}_f > 0$ implies an increase in transfer time lower the costs.

These are the criterion or optimality conditions for adding an initial or final coast that could lower the transfer cost by examining the algebraic signs of the gradients in the equation. The section elaborates more on this criterion that was applied in MMX transfer analysis.

3.2. Citerion for adding midcourse impulse

Primer vector theory also suggests that besides allowing the initial and final coasting times, adding one or more midcourse maneuvers would lower the cost of impulsive transfer trajectory [15]. In a practical scenario, adding mid-impulse is more challenging than allowing the spacecraft to coast in initial and final orbits, mainly due to the actual position and time of impulse being unknown. Fig. 8 illustrates two-impulse transfer trajectory with mid-course impulse (ΔV_{Mid}) at time t_m and position r_m: where $v_{m,a}$ and $v_{m,d}$ are velocity vector of arrival and the departing trajectory where the mid-course maneuver would take place.

The transfer cost due to adding midcorse impulse is given by adding midcourse velocity change magnitude ΔV_{Mid} to Eq. (32)

$$dJ = \boldsymbol{p}_0^T d\boldsymbol{\Delta V}_{Dep} + \Delta V_{Mid} + \boldsymbol{p}_f^T d\boldsymbol{\Delta V}_{Arr}, \tag{38}$$

where from [15],

$$dJ = \Delta V_{Mid} \left(1 - \boldsymbol{p}_m^T \frac{\boldsymbol{\Delta V}_{Mid}}{\Delta V_{Mid}}\right). \tag{39}$$

If the numerical value of this dot product is greater than one, $dJ < 0$ and the perturbed trajectory has a lower transfer cost than that of the nominal transfer trajectory. This suggest the criterion that explains when the addition of midcourse impulse would lower the transfer cost.

1. If p is greater than unity along the transfer trajectory, adding a midcourse impulse at a time when $p > 1$ reduces the transfer cost.

In this study, we have adapted these criteria to optimize the MMX transfer trajectories in the mission's proximity phase. The next two sections explain the methodology used to extract the suitable initial guesses for the trajectory optimization process.

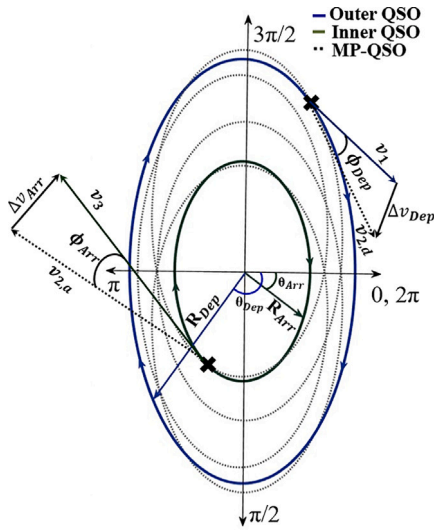

Fig. 9. Transfer method using intermediate QSOs.

4. Methods and initial guess computation

This section briefly introduces transfer methodology utilizing the bifurcated families of QSOs to explore the Martian moon, Phobos, to compute initial guesses for trajectory optimization. The interested reader may find additional details on the transfer methodologies in Refs. [7,12], respectively that uses the families of bifurcated QSOs to connect relative QSOs.

To extract the initial guesses, firstly, we design transfer trajectories utilizing the in-plane bifurcated families of QSOs (MP-QSO) [7]. Transfer maps computed using MP-QSO provide a basis for robust retrograde transfer trajectories around Phobos. Even if the spacecraft skips the ΔV maneuver at the designated point, the spacecraft remains in the MP-QSO, and later crossings can be used to perform the orbit injection into the target orbit. This method involves two impulse transfers, one to escape the initial QSO and another to insert into the desired lower altitude orbit. The necessary condition for utilizing MP-QSO for transfer applications is that the candidate $d : n$ MP-QSO must intersect both the departure and arrival orbits at least once and without intermediate maneuvers. We allow the departure and arrival point to vary across all possible longitudes $\theta = \arctan(-y/x)$ around Phobos as illustrated in Fig. 9. Subsequently, the whole transfer design space via MP-QSO is explored and used to develop overall transfer maps between pairs of QSO orbits accounting for multiple departure and arrival points. By inspection of computed transfer maps, combinations of departing and arrival longitudes that yield lower ΔV costs for the transfers are revealed. let $\boldsymbol{v}_{2,d}$ and $\boldsymbol{v}_{2,a}$ be the velocity vectors of a candidate MP-QSO at arbitrary departure and arrival points as illustrated in Fig. 9. The ΔV_{Dep} and ΔV_{arr} for the transfer can be represented as

$$\Delta V_{Dep} = \sqrt{v_{2,d}^2 + v_1^2 - 2v_1 v_{2,d} cos\phi_{Dep}}, \tag{40a}$$

$$\Delta V_{Arr} = \sqrt{v_{2,a}^2 + v_3^2 - 2v_1 v_{2,a} cos\phi_{Arr}}, \tag{40b}$$

where, $\boldsymbol{v}_1$ and $\boldsymbol{v}_3$ are the velocities of a spacecraft in the departing and arrival QSOs when maneuvers are executed. ϕ_{Dep} and ϕ_{Arr} represent the differences in the flight-path angles before and after the departing and arrival maneuvers.

Let us now denote C_1, C_3, and C_2 the Jacobi integrals of the departing QSOs, the arrival QSOs, and the transfer MP-QSO, respectively. Following Eq. (9), we have,

$$v_1^2 = 2(\mathcal{W}(\boldsymbol{r_1}) - C_1), \tag{41a}$$

$$v_{2,d}^2 = 2(\mathcal{W}(\boldsymbol{r_1}) - C_2), \tag{41b}$$

Table 3
MMX Transfer cases and initial guesses.

Transfer	Case	Transfer map	ΔV m/s	TOF (h)
QSO-H→QSO-M	1	1:7 MP-QSO	11.72	4.37
	2	1:10 MP-QSO	11.63	4.25
QSO-M→QSO-La	3	1:4 MP-QSO	3.99	3.81
	4	2:9 MP-QSO	4.15	5.21
QSO-La→QSO-Lb	5	3:10 MP-QSO	6.67	18.95
	6	1:3 MP-QSO	1.74	2.84
QSO-Lb→QSO-Lc	7	1:3 MP-QSO	2.2	1.47
	8	3:8 MP-QSO	0.97	6.3

$$v_{2,a}^2 = 2(\mathcal{W}(\boldsymbol{r_3}) - C_2), \tag{41c}$$

$$v_3^2 = 2(\mathcal{W}(\boldsymbol{r_3}) - C_3), \tag{41d}$$

implying

$$\Delta V_{Dep} = \sqrt{2(\mathcal{W}(\boldsymbol{r_1}) - C_1) + 2(\mathcal{W}(\boldsymbol{r_1}) - C_2) - 2v_1 v_{2,d} cos\phi_{Dep}}, \tag{42a}$$

$$\Delta V_{Arr} = \sqrt{2(\mathcal{W}(\boldsymbol{r_3}) - C_3) + 2(\mathcal{W}(\boldsymbol{r_3}) - C_2) - 2v_1 v_{2,a} cos\phi_{Arr}}. \tag{42b}$$

Note that $(\mathcal{W}(\boldsymbol{r}_1) - C_2)$ and $(\mathcal{W}(\boldsymbol{r}_3) - C_2)$ must be greater than zero otherwise the spacecraft cannot reach the corresponding quasi-satellite orbit. As a result, the ΔV_{total} of the transfer may be written as

$$\Delta V_{total} = \sqrt{4\mathcal{W}(\boldsymbol{r_1}) - 2(C_1 + C_2) - 2v_1 v_{2,d} cos\phi_{Dep}} + \sqrt{4\mathcal{W}(\boldsymbol{r_3}) - 2(C_3 + C_2) - 2v_1 v_{2,a} cos\phi_{Arr}}. \tag{43}$$

Eq. (43) illustrates how the minimum of ΔV_{total} may be affected by the effective potentials $\mathcal{W}(\boldsymbol{r}_1)$ and $\mathcal{W}(\boldsymbol{r}_3)$ of the departing and arrival QSOs; the possible values of C_2; the differences in the departing and arrival flight-path angles (ϕ_{Dep}, and ϕ_{Arr}, respectively).

Following [7], here are two examples of transfer maps between MMX baseline orbits shown in Fig. 10 along with the minimum ΔV transfer trajectory between QSO-H and QSO-M baseline orbits and Fig. 11 with transfer map using 3:8 family connecting QSO-Lb and QSO-Lc baseline orbits.

Transfer maps computed via MP-QSOs reveal the suitable longitudes at the departing (x-axis) and arrival (y-axis) QSOs around Phobos with ΔV_{total} of the transfers. Note that the transfer map patterns produced by the combination of departing and arrival QSOs are unique with respect to the MP-QSO used for the transfer. Initial guesses computed using the transfer method for different MMX baseline orbits are tabulated in Table 3, which is further optimized in the next section. In Table 3, we present the results of the MMX transfer simulations [7], where the transfer costs of QSO-Lb and QSO-Lc are notably low (approximately 1 m/s). These low values are primarily a result of the transfers being conducted via multi-revolutional Quasi-Satellite Orbits (MP-QSOs). This approach offers a significant advantage in terms of stability and robustness. Specifically, in the case of missed or inaccurate thrust maneuvers, the spacecraft remains within the same MP-QSO. This allows for later crossing points to be utilized for orbit insertion without requiring substantial additional ΔV. The multi-revolutional nature of the QSOs ensures that the spacecraft continues to follow a stable trajectory, maintaining proximity to the intended orbit. As a result, any minor deviations from the nominal trajectory due to thrust errors are naturally corrected through subsequent revolutions, offering flexibility in timing the orbital insertion. This inherent robustness, combined with the flexibility of multi-revolutional QSOs, as detailed in our previous work [6,7], demonstrates the effectiveness of this method for minimizing fuel costs while maintaining stable and reliable transfer trajectories.

5. Primer vector analysis for MMX baseline QSO transfer

This subsection analyzes the initial transfer trajectories computed from our transfer method by applying impulse primer vector theory.

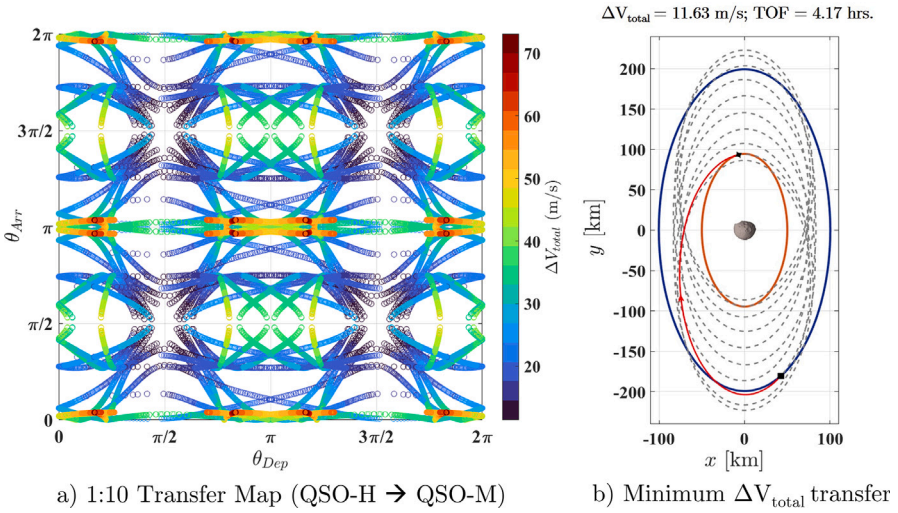

Fig. 10. QSO-H to QSO-M transfers via 1:10 MP-QSO.

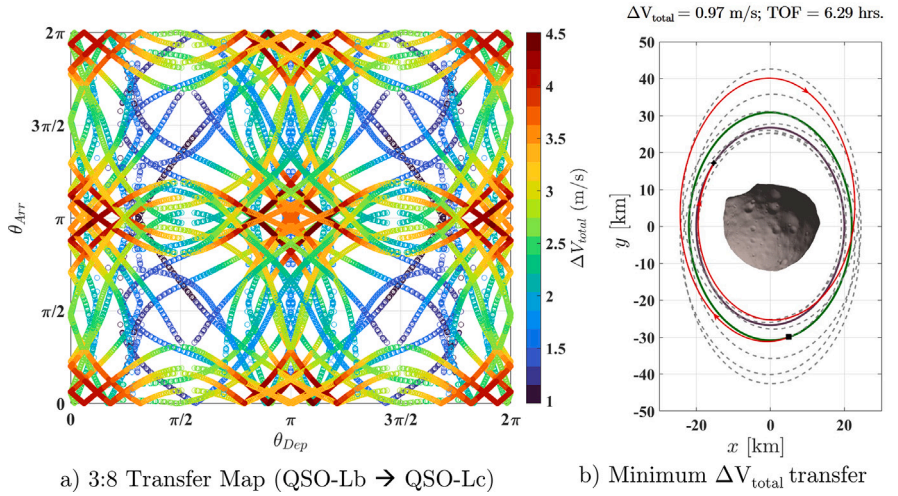

Fig. 11. QSO-Lb to QSO-Lc transfers via 3:8 MP-QSO.

Initially, we map the primer vector magnitude and its derivative of the initial minimum ΔV cases from Table 3. The evaluation shows that primer vector magnitude history along the transfer trajectories for some cases of transfers is greater than unit magnitude.i.e., $p > 1$, and primer vector derivatives history suggest that the $\dot{p}$ at the impulse locations are either $\dot{p} > 0$ or $\dot{p} < 0$. These initial impulse transfer solution evaluations indicate that they do not satisfy the necessary conditions for an optimal impulse transfer trajectory. Therefore, we introduce terminal coasting times and mid-course impulses to achieve optimal transfers [15].

To begin the optimization process, firstly, we use the initial conditions from the MP-QSO transfer maps as the first guess of the optimization problem. We allow the departure and arrival points on the relative QSOs to vary across all possible longitudes $\theta = \arctan(-y/x)$ around Phobos and iterate until the cost function ($\Delta V = \Delta V_{Dep} + \Delta V_{Arr}$) is minimized using a sequential quadratic programming algorithm.

The resulting optimal two-impulse transfer trajectories are plotted in red throughout the transfer cases. On evaluating the primer vector history of these optimal two-impulse trajectories, we find that most transfer trajectories satisfy the optimality condition on the primer vector derivative. However, the primer vector magnitude is greater than unity, suggesting room for improvement. Therefore, we further introduce a midcourse maneuver ΔV_{Mid} parallel to $\boldsymbol{p}_m$ and time (t_m) when primer vector magnitude is at its maximum (p_{max}). We reoptimize the transfer results utilizing this achieved position and time for midcourse impulse as an initial guess. We find significant changes in the transfer costs and resulting trajectories satisfy the necessary conditions for optimal impulse transfer trajectories. Figs. 12 to 15 illustrates our primer vector analysis results obtained for MMX candidate transfer cases listed in Table 3. In the case of QSO-H to M transfer cases shown in Fig. 12, using the initial guess from 1:7 and 1:10 MP-QSO transfer maps, the ΔV costs of 11.72 m/s and 11.63 m/s are reduced to 5.68 m/s with a midcourse maneuver. We choose the initial guess computed from the 1:4 and 2:9 MP-QSO transfer maps that suggested minimum ΔV transfers for QSO-M to La transfer. As shown in Fig. 13, the optimal total ΔV cost of transfers is lowered by ΔV from 4 m/s to 2.18 m/s in cases 3 and 4. Interestingly from Figs. 14 and 15, it can be noted that transfer cases 6 and 7 using the initial guesses (black) from 1:3 MP-QSO transfer maps suggest that primer vector magnitude is less than unity throughout the transfer. However, while examining the primer vector derivatives at impulse times, they fail to satisfy the optimality condition. In both cases 6 and 7, $\dot{p}_0 < 0$ indicates an earlier impulse time lowering the transfer cost, and $\dot{p}_0 > 0$ suggests an

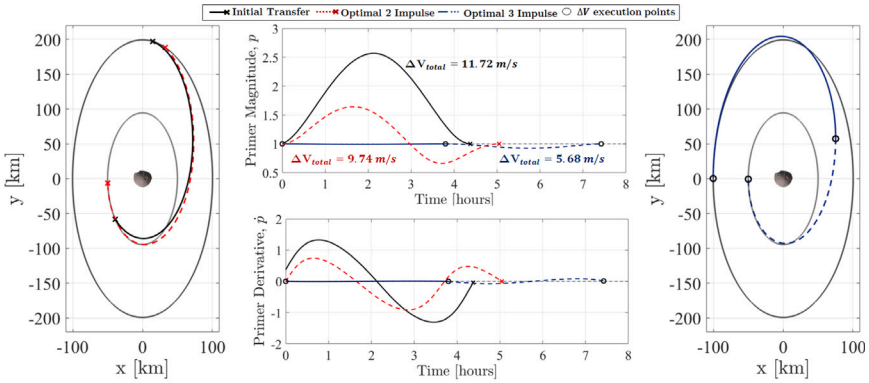

(a) Case 1

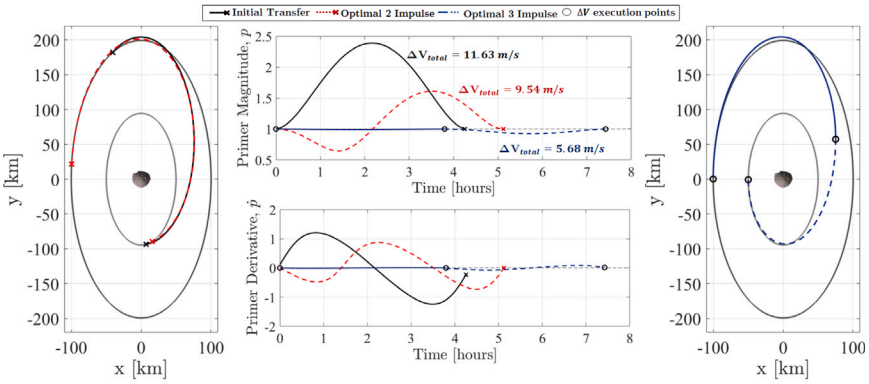

(b) Case 2

Fig. 12. (a) QSO-H→QSO-M using initial guess from 1:7 MP-QSO transfer map. (b) QSO-H→QSO-M using initial guess from 1:10 MP-QSO transfer map.

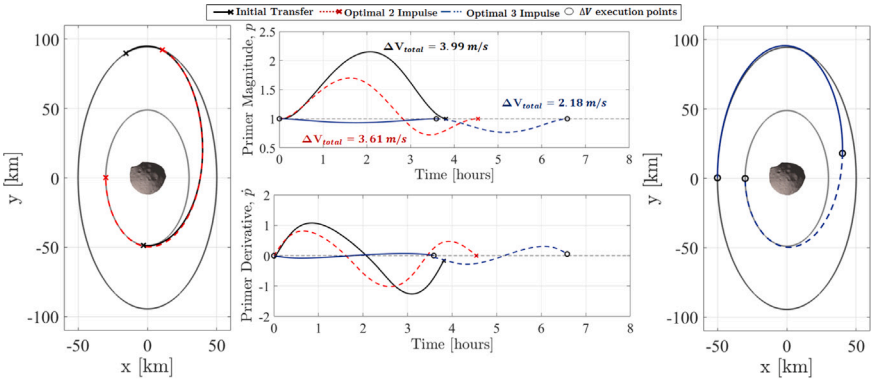

(a) Case 3

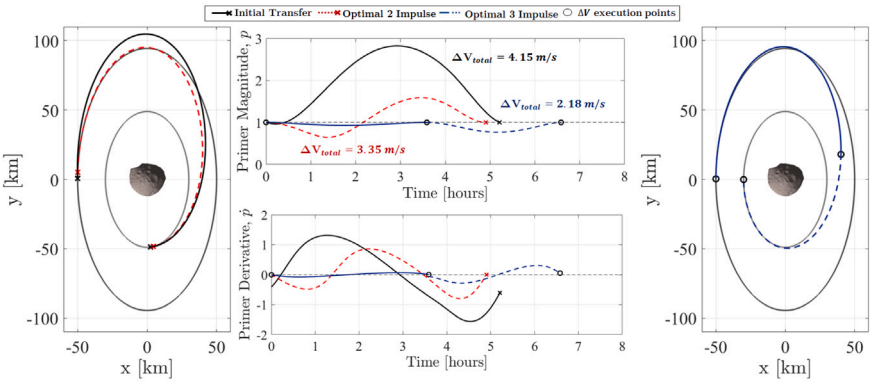

(b) Case 4

Fig. 13. (a) QSO-M→QSO-La using initial guess from 1:4 MP-QSO transfer map. (b) QSO-M→QSO-La using initial guess from 2:9 MP-QSO transfer map.

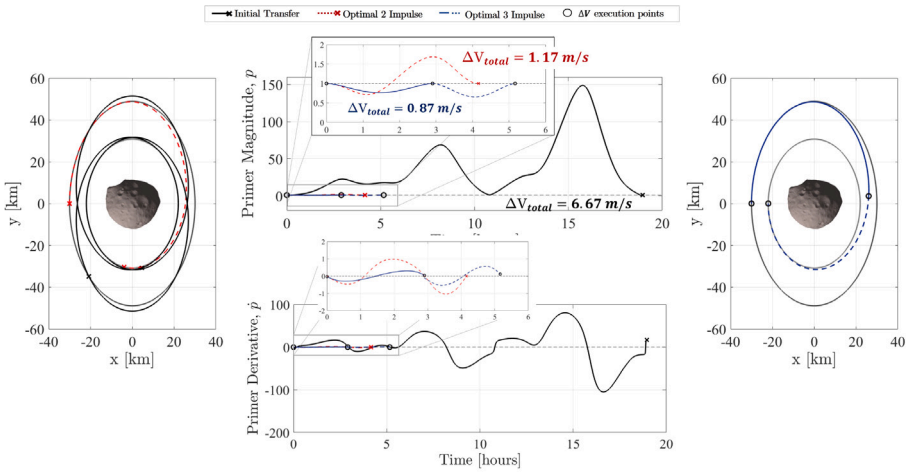

(a) Case 5

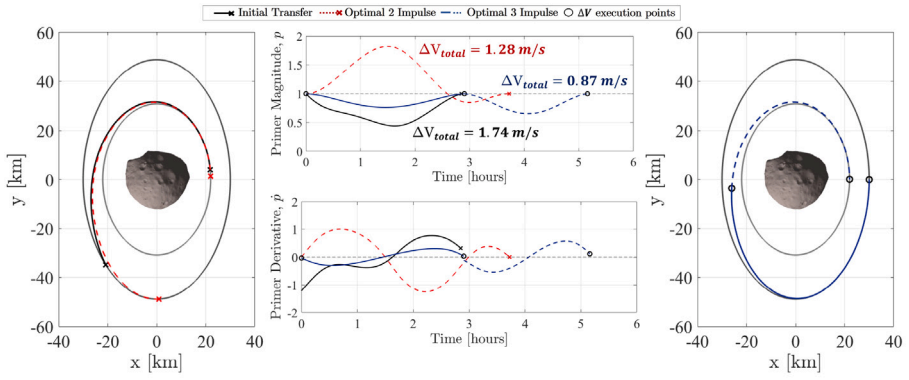

(b) Case 6

Fig. 14. (a) QSO-La→QSO-Lb using initial guess from 3:10 MP-QSO transfer map. (b) QSO-La→QSO-Lb using initial guess from 1:3 MP-QSO transfer map.

Table 4
Transfer summary.

Transfer	Optimal 2-impulse		Optimal 3-impulse	
Case	ΔV m/s	TOF (h)	ΔV m/s	TOF (h)
1	9.74	5.04	5.68	7.42
2	9.54	5.12	5.68	7.42
3	3.61	4.54	2.18	6.58
4	3.35	4.9	2.18	6.58
5	1.17	4.16	0.87	5.16
6	1.28	3.72	0.87	5.16
7	0.31	3.21	0.24	1.68
8	0.49	4.17	0.24	1.68

increase in transfer time that could lower the transfer cost. Numerical simulation shows that the increase in overall time of transfer and an earlier impulse reduced the transfer cost of the two-impulse transfers. We note that primer vector magnitude of the two-impulse transfers are not optimal and addition of midcourse impulse reduced the transfer cost.

On the other hand, cases 5 and 8 with initial guesses from 3:10 and 3:8 MP-QSO transfer maps for multi-revolution transfers between QSO-La→QSO-Lb and QSO-Lb→QSO-Lc also suggest that adding a midcourse impulse lowers the total ΔV cost of the respective transfers. The key finding of this analysis is that for all of these transfer cases, the departure and arrival points for optimal three-impulse transfer trajectories are on the same periapsis side. However, this is not the case with two-impulse transfers.

A summary of impulsive transfer cases in the Table 4 shows that introducing a midcourse impulse has improved the optimized total ΔV of all the MMX transfer cases. In the case of QSO-H→M transfers, there is a 51% improvement of 6 m/s from the initial guess. Similarly, optimal transfer results of QSO-M→La cases suggest a 47% improvement of the total ΔV costs. On the other hand, we see a significant improvement in total ΔV costs of about 50%–86% during QSO-La→Lb transfer and 75%–87% improvement in QSO-Lb→Lc transfers.

6. Conclusion

In summary, the present study aimed at optimizing transfer trajectories connecting relative quasi-satellite orbits in the vicinity of Phobos. Accordingly, we considered the Hill Problem with an ellipsoidal gravity model to investigate the QSOs transfers utilizing the bifurcated families of QSOs. We applied impulsive primer vector theory to optimize these transfer trajectories such that they meet optimality conditions. In particular, we analyzed transfers between MMX candidate orbits and found that introducing terminal coasting and midcourse impulse reduces the initial transfer cost. We also highlight our key finding in relative retrograde orbital transfers: the departure and arrival points lie on the same side as a periapsis point for the optimal three-impulse transfers. Such a conclusion contributes in several ways to our understanding of the dynamical environment around Phobos and provides a basis for the selection of transfer ΔV execution points for transfer designs in higher-fidelity models of the Martian system. Moreover, future missions seeking lower-ΔV transfer opportunities between stable retrograde orbits around Phobos or any small irregular planetary satellites in the solar system could use the transfer methodology and evaluation presented in this research.

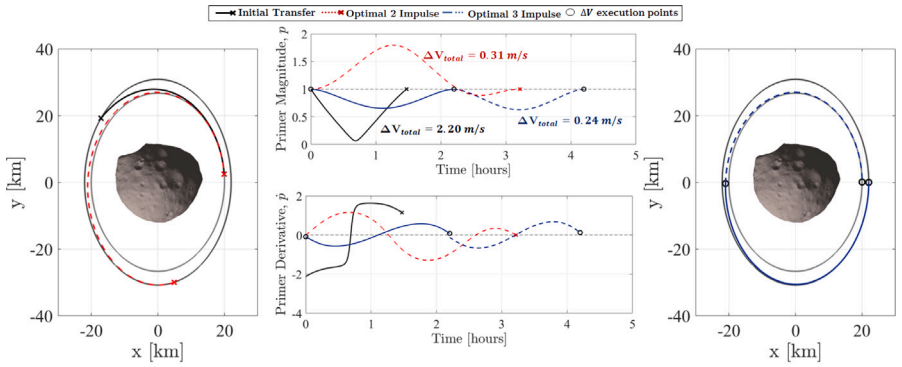

(a) Case 7

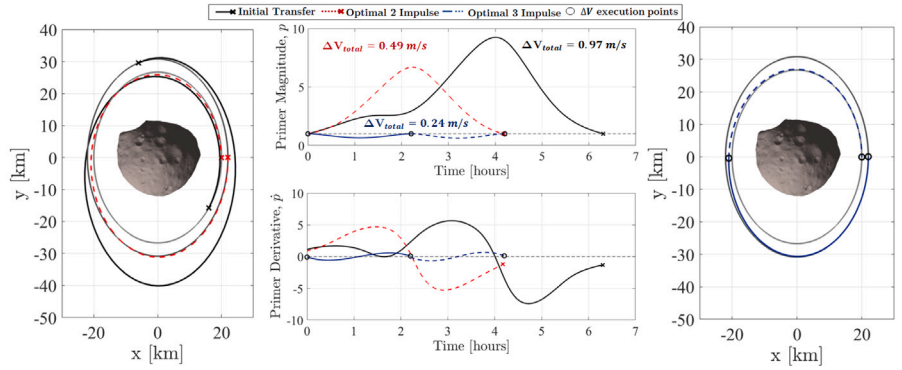

(b) Case 8

Fig. 15. (a) QSO-Lb→QSO-Lc using initial guess from 1:3 MP-QSO transfer map. (b) QSO-Lb→QSO-Lc using initial guess from 3:8 MP-QSO transfer map.

CRediT authorship contribution statement

Nishanth Pushparaj: Writing – original draft, Project administration, Methodology, Investigation, Formal analysis, Data curation, Conceptualization. **Nicola Baresi:** Writing – review & editing, Supervision. **Yasuhiro Kawakatsu:** Supervision.

Declaration of competing interest

The authors declare that they have no known competing financial interests or personal relationships that could have appeared to influence the work reported in this paper.

Acknowledgments

Nishanth Pushparaj was supported by the MEXT (Ministry of Education, Culture, Sports, Science and Technology), Japan research scholarship from the Japanese government during this study. Part of this research is also supported by the University of Nottingham. The authors appreciate the helpful comments of the reviewers and the Editor.

References

[1] R.I. Citron, H. Genda, S. Ida, Formation of phobos and deimos via giant impact, Icarus 252 (2015) 334–338.
[2] M. Pajola, M. Lazzarin, C.M. Dalle Ore, D.P. Cruikshank, T.L. Roush, S. Magrin, I. Bertini, F. La Forgia, C. Barbieri, Phobos as a D-type captured asteroid, spectral modeling from 0.25 to 4.0μm, Astrophys. J. 777 (2013) 127.
[3] Y. Kawakatsu, K. Kuramoto, T. Usui, H. Ikeda, K. Yoshikawa, H. Sawada, N. Ozaki, T. Imada, H. Otake, K. Maki, M. Otsuki, R. Muller, K. Zacny, Y. Satoh, S. Mary, M. Grebenstein, A. Tokaji, L. Yuying, F. Gonzalez-Franquesa, N. Pushparaj, T. Chikazawa, System definition of Martian Moons Exploration (MMX), in: 71st International Astronautical Congress, IAC 2020, Virtual, Online, 12-14 2020.
[4] Y. Kawakatsu, K. Kuramoto, T. Usui, H. Sugahara, H. Ootake, R. Yasumitsu, K. Yoshikawa, S. Mary, M. Grebenstein, H. Sawada, T. Imada, T. Shimada, K. Ogawa, M. Otsuki, M. Baba, K. Fujita, K. Zacny, D. van Dyne, Y. Satoh, A. Tokaji, Preliminary design of Martian Moons eXploration (MMX), Acta Astronaut. 202 (2023) 715–728.
[5] D.J. Scheeres, S. Van Wal, Z. Olikara, N. Baresi, Dynamics in the Phobos environment, Adv. Space Res. 63 (2019) 476–495.
[6] K. Ichinomiya, N. Baresi, Y. Kawakatsu, T. Yanao, Quasi-satellite orbit transfers via multi-revolutional periodic orbits, in: AAS/AIAA Space Flight Mechanics Meeting, Hawaii, USA, 2019.
[7] N. Pushparaj, N. Baresi, K. Ichinomiya, Y. Kawakatsu, Transfers around Phobos via bifurcated retrograde orbits: Applications to Martian Moons eXploration mission, Acta Astronaut. 181 (2021) 70–80.
[8] Y. Liang, N. Pushparaj, Y. Kawakatsu, Point-to-point jumping transfer on phobos by prograde g' family, J. Guid. Control Dyn. 45 (6) (2022) 1172–1183.
[9] E. Canalias, L. Lorda, E. Hekma, Transfer between planar and three-dimensional quasi satellit orbits in the vicinity of Phobos, in: AAS/AIAA Space Flight Mechanics Meeting, Hawaii, USA, 2019.
[10] H. Chen, E. Canalias, D. Hestroffer, X. Hou, Effective stability of quasi-satellite orbits in the spatial problem for phobos exploration, J. Guid. Control Dyn. 43 (2020) 2309–2320.
[11] N. Pushparaj, N. Baresi, Y. Kawakatsu, Design of transfer trajectories between planar and spatial quasi-satellite orbits, in: AIAA SciTech 2020 Forum, Orlando, Florida, USA, 2020.
[12] N. Pushparaj, N. Baresi, Y. Kawakatsu, Transfers and orbital maintenance of spatial retrograde orbits for Phobos exploration, Acta Astronaut. 189 (2021) 452–464.
[13] J.E. Prussing, Primer Vector Theory and Applications, in: Cambridge Aerospace Series, Cambridge University Press, 2010, pp. 16–36.
[14] R.P. Russell, Primer vector theory applied to global low-thrust trade studies, J. Guid. Control Dyn. 30 (2) (2007) 460–472.
[15] P.M. Lion, M. Handelsman, Primer vector on fixed-time impulsive trajectories, AIAA J. 6 (1) (1968) 127–132.
[16] D.F. Lawden, Optimal Trajectories for Space Navigation, Butterworths, London, 1963.
[17] J.E. Prussing, J.H. Chiu, Optimal multiple-impulse time-fixed rendezvous between circular orbits, J. Guid. Control Dyn. 9 (1) (1986) 17–22.
[18] L. Casalino, G. Colasurdo, D. Pastrone, Optimization procedure for preliminary design of opposition-class Mars missions, J. Guid. Control Dyn. 21 (1) (1986) 134–140.

[19] K.J. Zhu, J.F. Li, H.X. Baoyin, Satellite scheduling considering maximum observation coverage time and minimum orbital transfer fuel cost, Acta Astronaut. 66 (1–2) (2010) 220–229.
[20] X.Y. Li, D. Qiao, H.B. Chen, Interplanetary transfer optimization using cost function with variable coefficients, Astrodynamics 3 (2) (2019) 173–188.
[21] L.A. Hiday-Johnston, K.C. Howell, Transfers between liberation-point orbits in the elliptic restricted problem, Celest. Mech. Dyn. Astron. 58 (4) (1994) 317–337.
[22] K.E. Davis, R.L. Anderson, D.J. Scheeres, G.H. Born, Optimal transfers between unstable periodic orbits using invariant manifolds, Celest. Mech. Dyn. Astron. 109 (3) (2011) 241–264.
[23] K.A. Bokelmann, R.P. Russell, Optimization of impulsive europa capture trajectories using primer vector theory, J. Astronaut. Sci. 67 (2) (2020) 485–510.
[24] D. Jezewski, Primer vector theory applied to the linear relative-motion equations, Optim. Control Appl. Methods 1 (4) (1980) 387–401.
[25] S. Shuster, D. Geller, M. Harris, Analytic impulsive maneuver sequences for nominal safety ellipse reconfigurations, J. Guid. Control Dyn. 43 (10) (2020) 1837–1853.
[26] M. Zheng, J. Luo, Z. Dang, Optimal impulsive rendezvous for highly elliptical orbits using linear primer vector theory, Chinese J. Aeronaut. 37 (3) (2024) 194–207.
[27] G. Bucchioni, G. Gemignani, F. Lombardi, A. Bellome, J.P.F. Leitao, S. Lizy-Destrez, M. Innocenti, Optimal time-fixed impulsive non-keplerian orbit to orbit transfer algorithm based on primer vector theory, Commun. Nonlinear Sci. Numer. Simul. 124 (2023) 107307.
[28] M. Rebelo, J.P. Sanchez, Optimizing launch window opportunities for ESA's comet intercepter mission using primer vector theory, Acta Astronaut. 219 (2024) 340–352.
[29] W.D. MacMillan, The Theory of the Potential, McGraw-Hill, New York, 1930.
[30] D.J. Scheeres, Dynamics about uniformely rotating triaxial Ellipsoids: Applications to Asteroids, ICARUS 110 (1994) 225–238.
[31] K. Willner, X. Shi, J. Oberst, Phobos' shape and topography models, Planet. Space Sci. 102 (2014) 51–59.
[32] A. Wintner, The Analytical Foundations of Celestial Mechanics, Princeton University Press, Princeton, NJ, 1947.
[33] D.J. Scheeres, Orbital Motion in Strongly Perturbed Environments, Springer-Verlag Berlin, 2012.
[34] W.H. Press, S.A. Teukolsky, W.T. Vetterling, B.P. Flannery, Numerical Recipes: The Art of Scientific Computing, third ed., Cambridge University Press, 2007.
[35] H.D. Mittelmann, A pseudo-arclength continuation method for nonlinear eigenvalue problems, SIAM J. Numer. Anal. 23 (1986) 1007–1016.
[36] H. Ikeda, S. Mitani, Y. Mimasu, G. Ono, K. Nigo, Y. Kawakatsu, Orbital operations strategy in the vicinity of Phobos, in: 31st International Symposium on Space Technology and Science, Matsuyama, Japan, 2017.
[37] R. Broucke, Stability of periodic orbits in the elliptic, restricted three-body problem, AIAA Journal. 7 (6) (1969) 1003–1009.
[38] V.V. Markellos, Numerical investigation of the planar restricted three-body problem, I. Periodic orbits of the second generation in the Sun-Jupiter System, Celest. Mech. 9 (3) (1974) 365–380.
[39] M. Lara, R. Russell, B.F. Villac, Classification of the Distant Stability Regions at Europa, J. Guid. Control Dyn. 30 (2007) 409–418.